We are IntechOpen, the world's leading publisher of Open Access books Built by scientists, for scientists

4,800
Open access books available

122,000
International authors and editors

135M
Downloads

Our authors are among the

154
Countries delivered to

TOP 1%
most cited scientists

12.2%
Contributors from top 500 universities

CLARIVATE ANALYTICS BOOK CITATION INDEX INDEXED

WEB OF SCIENCE™

Selection of our books indexed in the Book Citation Index in Web of Science™ Core Collection (BKCI)

Interested in publishing with us?
Contact book.department@intechopen.com

Numbers displayed above are based on latest data collected.
For more information visit www.intechopen.com

10

Optical Solitons from a Photonic Crystal Fiber and Their Applications

Naoki Karasawa and Kazuhiro Tada
Chitose Institute of Science and Technology
Japan

1. Introduction

A photonic crystal fiber (PCF) is a fiber that contains the regular (usually hexagonal) arrays of air holes in the propagation direction of an optical fiber. At the center position, the core is created by not making an air hole and the light wave propagates at the core position since the effective refractive index of the core is higher than that of the photonic crystal clad surrounding the core. Photonic crystal fibers of this type have been used to generate ultrabroadband optical pulses by propagating femtosecond optical pulses in these fibers (Ranka et al., 2000). The core diameter of a PCF for the generation of ultrabroadband optical pulses using a Ti:sapphire laser (center wavelength ∼800 nm) is about 1-2 μm if it is assumed that the silica core is surrounded by regular air holes. Due to the waveguide dispersion, the group velocity dispersion (GVD) becomes negative at 800 nm. Because of the small core diameter and the negative GVD, nonlinear effects are enhanced and optical solitons are generated in a PCF. Theoretical calculations for elucidating the mechanism of the ultrabroadband pulse generation in a PCF have been performed (Husakou & Herrmann, 2001) and the generation of fundamental soliton pulses by the fission of an input higher-order soliton pulse due to the third and higher order dispersion as well as the higher-order nonlinear effects including the Raman effects are found to be important for the spectral broadening. Supercontinuum generation in a PCF is reviewed in (Dudley et al., 2006). The center wavelength of the generated fundamental soliton pulse becomes longer as it propagates in a PCF due to soliton self-frequency shift and its center wavelength can be changed by the peak power or the chirp of an input pulse. Recently, it was used as a variable-wavelength light source in various applications including coherent anti-Stokes Raman scattering (CARS) spectroscopy and optical coherence tomography (OCT). The present article describes the properties of the fundamental solitons from a PCF and its applications studied in our laboratory.

2. Fundamental soliton pulse

It is well known that the soliton pulse, which does not change its shape as it propagates in a fiber, can be created when the pulse propagates in the anomalous dispersion region (Agrawal, 2007; Hasegawa, 1992). If we consider the electric field (considered to be scalar) that depends on only time t and propagation position z such that $E(z,t) = Re[A(z,t)e^{i(\beta_0 z - \omega_0 t)}]$, where Re shows the real part, ω_0 is the central angular frequency, and β_0 is the propagation constant at ω_0 ($\beta_0 = \beta(\omega_0)$) of a pulse, the slowly varying envelope approximation (SVEA) equation for

the envelope $A(z,t)$ (normalized to have the unit [$W^{1/2}$]) may be obtained from the Maxwell equation after various approximations (Karasawa et al., 2001) as follows,

$$\partial_\zeta A(\zeta,T) = -\frac{i}{2}\beta_0^{(2)}\partial_T^2 A(\zeta,T) + i\gamma(\omega_0)|A(\zeta,T)|^2 A(\zeta,T). \quad (1)$$

In this equation, the coordinates are transformed $\zeta = z$, $T = t - \beta_0^{(1)} z$ such that the pulse center is always at the time origin ($\beta_0^{(1)} = \partial_\omega \beta|_{\omega_0}$ is the inverse of the group velocity of the pulse). In the right hand side of Eq. 1, the first term arises from the dispersion, where the GVD is given by $\beta_0^{(2)} = \partial_\omega^2 \beta|_{\omega_0}$. The second term arises from the nonlinear self-phase modulation (SPM) with the frequency-dependent nonlinear coefficient $\gamma(\omega_0) = n(\omega_0) n_2^I(\omega_0)\omega_0^2(1-f_R)/(c^2\beta_0 A_{\rm eff}(\omega_0))$, where $n(\omega_0)$ and $n_2^I(\omega_0)$ are the linear and the nonlinear indices of refraction of a medium, c is the speed of light, $A_{\rm eff}(\omega_0)$ is the effective mode area in a fiber, and f_R is the contribution of the Raman term ($f_R \simeq 0.3$ for fused silica). When the GVD is negative and the input power is chosen appropriately, the effects of these terms on the variations of the envelope cancel, and a stable soliton pulse can be propagated. By changing the variables to dimensionless ones such that $\xi = \zeta/L_D$, $\tau = T/T_0$, $u(\xi,\tau) = \sqrt{\gamma(\omega_0)L_D}A(\xi,\tau)$ (Agrawal, 2007), where T_0 is the pulse width parameter, and $L_D = T_0^2/|\beta_0^{(2)}|$ is the dispersion length, we have

$$\partial_\xi u(\xi,\tau) = \frac{i}{2}\partial_\tau^2 u(\xi,\tau) + i|u(\xi,\tau)|^2 u(\xi,\tau), \quad (2)$$

when $\beta_0^{(2)} < 0$. This equation was solved by the inverse scattering method and has a fundamental soliton solution of a form (Agrawal, 2007)

$$u(\xi,\tau) = \eta \ \mathrm{sech}\ \eta(\tau + \delta\xi - \tau_s) e^{-i\delta\tau + i(\eta^2-\delta^2)\xi/2 + i\phi_s}, \quad (3)$$

where η and δ are determined by the eigenvalue of the inverse scattering problem, and τ_s and ϕ_s are constants. Here, ϕ_s can be included in an initial carrier wave phase, and δ and τ_s can be eliminated by shifting the carrier center frequency and the initial temporal position of the pulse. Therefore it can be written as $u(\xi,\tau) = \eta\ \mathrm{sech}\ (\eta\tau)e^{i\eta^2\xi/2}$, which shows that the envelope intensity does not change as it propagates in a fiber. The parameter η determines both the amplitude and the width of the soliton pulse. If the pulse width is T_0, $\eta = 1$ and the solution is given simply by $u(\zeta,\tau) = \ \mathrm{sech}\ (\tau)e^{i\xi/2}$. If the input pulse shape of a laser is approximated as $u(0,\tau) = B\ \mathrm{sech}\ \tau$, the number of eigenvalues N is given by $B - 1/2 < N \leq B + 1/2$ (Satsuma & Yajima, 1974). For an input pulse envelope with a peak power P_0, $A(0,T) = \sqrt{P_0}\ \mathrm{sech}\ (T/T_0)$ and this "soliton number" B becomes $B = \sqrt{P_0\gamma(\omega_0)L_D} = \sqrt{P_0\gamma(\omega_0)T_0^2/|\beta_0^{(2)}|}$. If B is exactly equal to N, the solution can be obtained in terms of N amplitudes $\eta_j = 1, 3, 5, ..., (2N-1)$. For $N \geq 2$, higher-order N-soliton solutions were found (Satsuma & Yajima, 1974; Schrader, 1995). These N-soliton solutions may be considered to be consisted of N single solitons (Schrader, 1995).

In the real fiber of our interest, neglected terms deriving Eq. 1, such as higher-order dispersion terms, self-steepening terms, and the Raman term become important. If we use a slowly-evolving wave approximation (SEWA) instead of SVEA, the following propagation

equation can be derived (Karasawa et al., 2001),

$$\partial_\zeta A(\zeta,T) = i(\hat{D}' + \hat{D}_{\rm corr})A(\zeta,T) + i\gamma'(\omega_0)(1+is\partial_T)\Big[(1-f_R)|A(\zeta,T)|^2 + \frac{2}{3}f_R\int_0^\infty h_R(T')|A(\zeta,T')|^2dT'\Big]A(\zeta,T), \quad (4)$$

where

$$\hat{D}' = \sum_{n=0}^{\infty}\frac{i^n}{n!}\Big(\partial_\omega^n(\beta(\omega)+\frac{i\alpha(\omega)}{2})|_{\omega_0}\Big)\partial_T^n - \beta_0 - i\beta_0^{(1)}\partial_T, \quad (5)$$

is the dispersion terms that contain all higher-order terms with $\alpha(\omega)$ to be the loss constant, $\hat{D}_{\rm corr} = (1+i\beta_0^{(1)}\partial_T/\beta_0)^{-1}\hat{D}'^2/(2\beta_0)$ is the dispersion correction term, $s = 2/\omega_0 - \beta_0^{(1)}/\beta_0 + \partial_\omega(\log(n(\omega)n_2^I(\omega)/A_{\rm eff}(\omega)))|_{\omega_0}$ is the self-steepening term, $\gamma'(\omega_0) = \gamma(\omega_0)/(1-f_R)$, and $h_R(T) = (\tau_1^2+\tau_2^2)e^{-T/\tau_2}\sin(T/\tau_1)/(\tau_1\tau_2^2)$ is the response function of the delayed Raman response with $\tau_1 = 12.2$ fs and $\tau_2 = 32$ fs for fused silica (Blow & Wood, 1989).

Because of the presence of extra terms not included in Eq. 1, the inputted pulse with $u(0,\tau) = B$ sech τ separates to multiple soliton pulses if the amplitude $B > 1.5$. The main reason of the splitting is the self-frequency shift due to the Raman effect (Gordon, 1986; Mitschke & Mollenauer, 1986), which depends on the pulse amplitude and width. If the center frequency is changed, the temporal delay of the pulse changes due to the dispersive effect ($\hat{D}'$ term). Independently, it is modified by the self-steepening effect (s term). The effects of these higher-order terms were investigated by moments equations for pulse parameters (Agrawal, 2007), where the variations of pulse parameters (pulse width, chirp, delay, and center angular frequency) were calculated as functions of propagation distance z. The variation of the center frequency of the fundamental soliton ($N = 1$) without a chirp can be approximated as

$$\omega_0(z) = -\frac{8T_R\gamma(\omega_0)P_0}{15T_0^2}z = -\frac{8T_R|\beta_0^{(2)}|}{15T_0^4}z, \quad (6)$$

where T_R is the first moment of the Raman response function, $T_R \simeq f_R\int_0^\infty th_R(t)dt = 2.4$ fs for fused silica. This wavelength-variable fundamental soliton pulse emits a phase-matched dispersive wave, which is the important mechanism for generating supercontinuum, especially for shorter wavelength components (Husakou & Herrmann, 2001).

In Fig. 1, the model structure of a PCF used in our experiment and the dispersion properties of the PCFs with different structural parameters calculated by a multipole method (Zolla et al., 2005) using two rings of air holes surrounding a core are shown. In Fig. 2, the variations of temporal and spectral pulse intensities are shown as a function of propagation distance z, where, Eq. 4 is solved numerically for a PCF with the dispersion property shown in Fig. 1 (b) with the pitch 1.07 μm and diameter 0.7 μm (NKT Photonics NL-1.5-590). In calculations, a Gaussian input pulse, with the full width at half-maximum (FWHM) width $T_p = 50$ fs, the peak power $P_0 = 4$ kW, and the center wavelength 800 nm, where the GVD is anomalous, was used. The fiber material was assumed to be fused silica with $n_2^I = 2.48\times10^{-20}$ m^2/W, and $A_{\rm eff} = 1.7671$ μm^2, which gave the soliton number N=5.03. The propagation loss and the derivative term in s were neglected in calculations. Also in Fig. 2, the spectrogram created by the calculation at propagation distances $z = 50$ mm and $z = 100$ mm are shown. From Fig. 2, we can see that three soliton pulses (S1, S2, and S3) are created in this case after about

$z = 25$ mm. The center frequency of the most intense fundamental soliton (S1) decreases until $z = 150$ mm, where GVD becomes zero. Because of this frequency shift, the group velocity decreases and the delay time becomes about 1000 fs at $z = 100$ mm. The pulse width, the spectral bandwidth, and the peak power of the most intense soliton are 14 to 18 fs, 60 to 65 nm, and 5 to 7 kW, respectively. Thus, this wavelength-variable fundamental soliton pulse has a shorter pulse width and a higher peak power compared with the inputted pulse. This soliton pulse emits a dispersive wave (D1) at the short wavelength near 550 nm, where the GVD is positive and its delay time increases quite rapidly. It is observed that there is a dispersive wave (D2) near 1400 nm after $z = 150$ mm. The intensities of other two soliton pulses (S2 and S3) are much weaker than the first soliton pulse (S1). The shift of the center frequency of the third soliton (S3) is small since its peak power is small. Also, it has a negative delay time since its center wavelength is shorter than 800 nm. From the spectrograms (c) and (d), we can see that three waves marked by S1, S2, and S3 are indeed localized pulses.

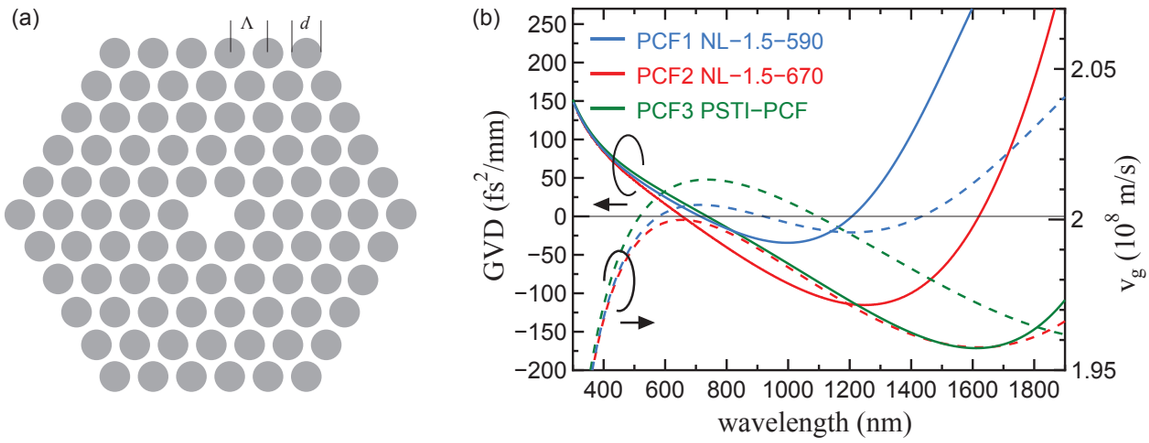

Fig. 1. (a) The structure of a five-ring PCF with a pitch Λ and a diameter d. Gray areas show air holes. (b) The GVD and the group velocity ($v_g = 1/\beta^{(1)}$) of the PCF shown in (a) calculated by a multipole method with various parameters. Blue curves show NKT Photonics NL-1.5-590 ($\Lambda = 1.07\mu$m, $d = 0.7\mu$m), red curves show NKT Photonics NL-1.5-670 ($\Lambda = 1.3\mu$m, $d = 1.105\mu$m), and green curves show PSTI-PCF ($\Lambda = 1.57\mu$m, $d = 1.31\mu$m).

3. Experiment on soliton properties

3.1 Soliton wavelength versus delay time

In the previous section, it is shown from calculations that an intense fundamental soliton pulse can be obtained by inputting a femtosecond pulse into a PCF and its center wavelength changes during propagation. However, in usual experiment, the length of a PCF is fixed and the center wavelength is controlled by modifying the input pulse parameters. In this section, the control of the center wavelength by the input pulse power and the delay property of a soliton are described.

As shown in Eq. 6, the variation of the center angular frequency due to self-frequency shift of a soliton pulse can be approximated to be proportional to the propagation distance z. This proportionality constant contains the peak power P_0 of the soliton pulse. Thus it is expected

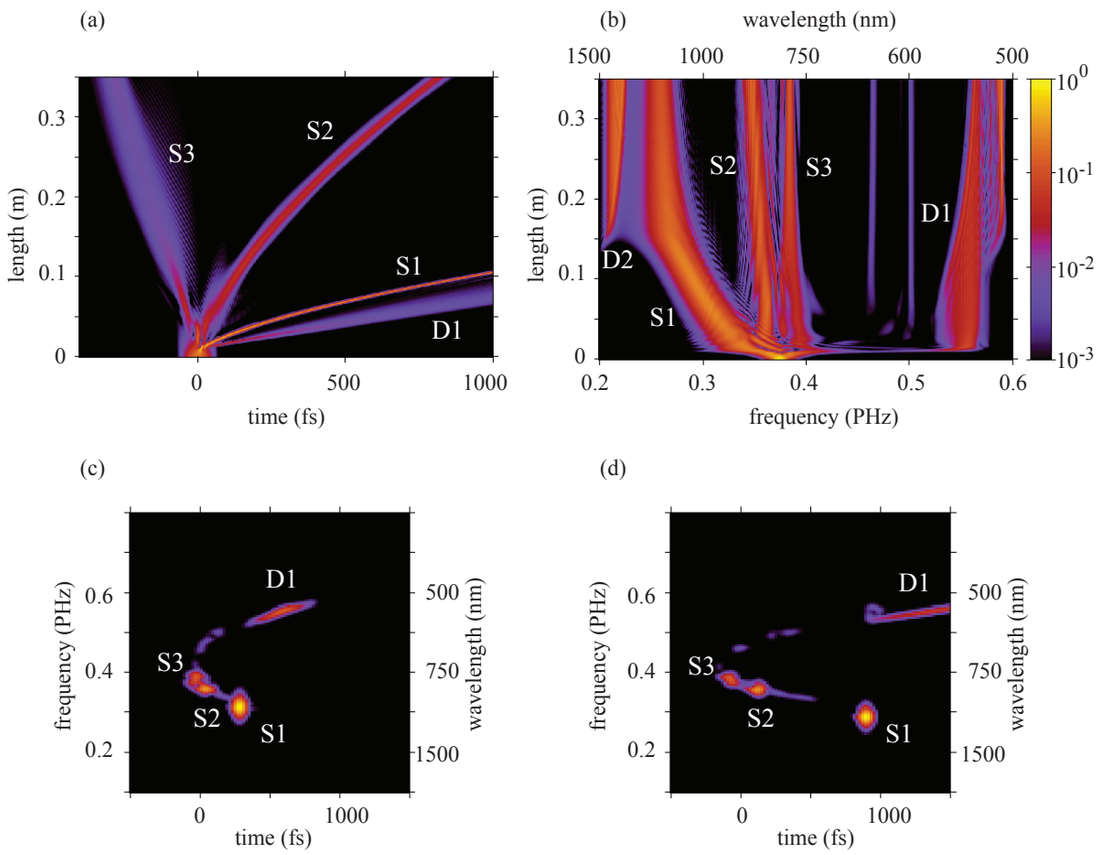

Fig. 2. The calculated temporal (a) and spectral (b) intensities of an optical pulse inputted in a PCF (NKT Photonics NL-1.5-590) versus distance. In (c) and (d), spectrograms at $z = 50$ mm (c) and $z = 100$ mm (d) are shown. S1, S2, and S3 show fundamental soliton pulses. D1 and D2 show the dispersive waves emitted from a soliton S1. The intensities are shown in a logarithmic scale.

that the amount of the shift is proportional to the power of the input pulse approximately. If the variation of the center angular frequency is proportional to the distance, the delay time of the soliton at the output end of a PCF can be estimated as follows. The propagation time $T(\omega_{0o})$ of a soliton with the angular frequency ω_{0o} at the output end of a PCF with a length L is given by

$$T(\omega_{0o}) = \int_0^L \beta^{(1)} dz = \frac{1}{K} \int_{\omega_{0i}}^{\omega_{0o}} \beta^{(1)} d\omega = \frac{1}{K}(\beta(\omega_{0o}) - \beta(\omega_{0i})), \tag{7}$$

where ω_{0i} is the center angular frequency at the input end and K is the proportional constant, which is given by $K = (\omega_{0o} - \omega_{0i})/L$. Thus, we have

$$T(\omega_{0o}) = \frac{\beta(\omega_{0o}) - \beta(\omega_{0i})}{\omega_{0o} - \omega_{0i}} L. \tag{8}$$

This equation shows that the delay time of the soliton for various center wavelengths can be estimated by the propagation constant $\beta(\omega)$ only. We have performed experiment to examine

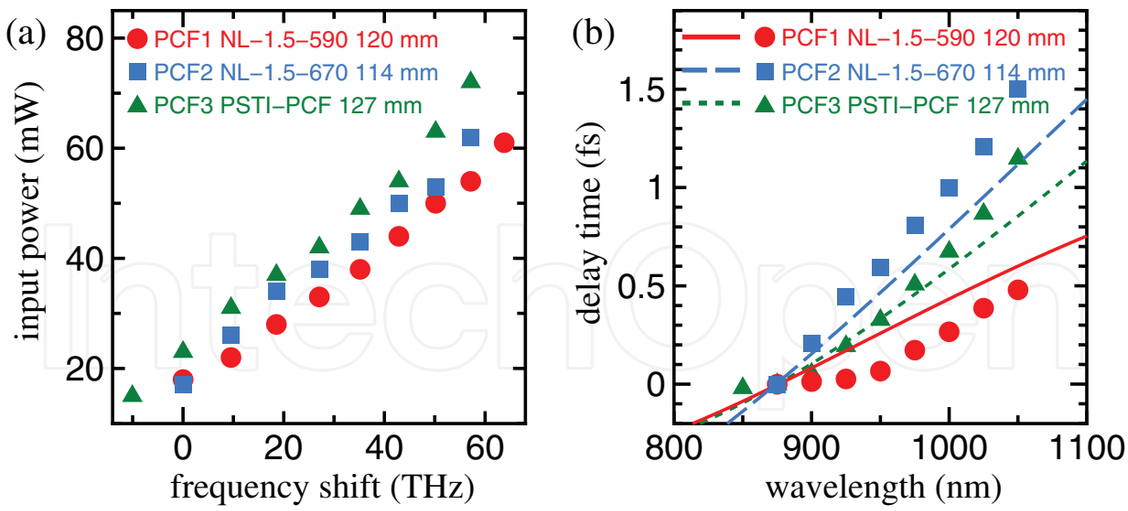

Fig. 3. (a) Frequency shift versus input power of soliton pulses for three different PCFs. (b) Wavelength versus delay time of soliton pulses for three different PCFs. Solid curves show delay times calculated by Eq. 8.

the dependence of the center wavelength and the delay time on the input power for three different PCFs, where the dispersion properties are shown in Fig. 1 (b). In experiment, a pulse from a Ti:sapphire laser oscillator (center wavelength 800 nm, pulse width 50 fs, repetition rate 78 MHz, and average power 620 mW) was propagated in PCFs, where the average power was controlled by a variable neutral density filter. In Fig. 3 (a), the frequency shifts of the most intense soliton pulses versus input pulse power are shown, where the shifts at 875 nm were set to be 0. As expected, the frequency shifts are almost proportional to the input pulse power for three different PCFs. In Fig. 3 (b), the delay times of the soliton pulses versus wavelength are shown and compared with delay times given in Eq. 8, where the delay times at 875 nm were set to be 0 and ω_{0i} was set to be $2\pi c/(800\text{ nm})$. It is seen that the approximate delay times for the PCFs were estimated correctly. The discrepancies are presumably due to the neglect of delay times required for the soliton fission near the input ends of the PCFs in Eq. 8.

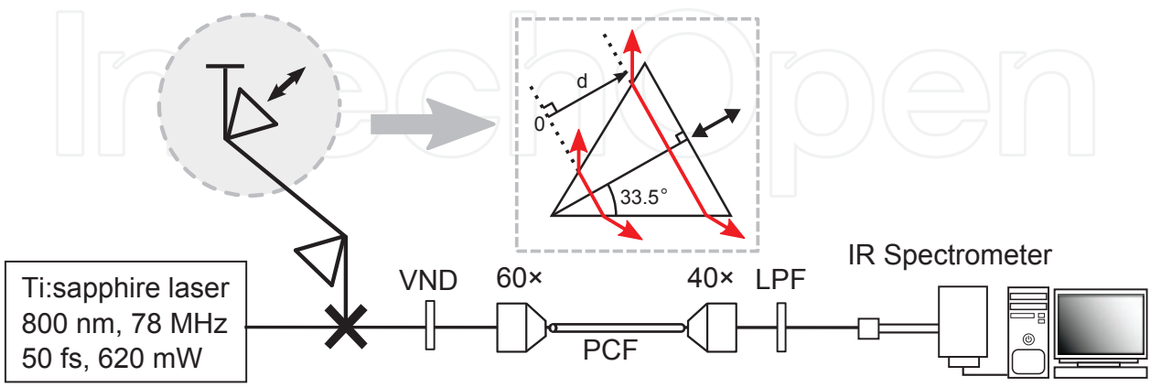

Fig. 4. Experimental setup for the control of a soliton by the chirp of an input pulse. Here, VND: variable neutral density filter, and LPF: long-wavelength pass filter.

3.2 Soliton wavelength control by chirp

We have studied the control of the soliton center wavelengths by the chirp of an input pulse (Karasawa et al., 2007; Tada & Karasawa, 2008). In experiment, the chirp of an input pulse was changed by varying the position of one of the prisms in a prism pair and the spectrum and the delay time of an output pulse from the PCF were measured. Experimental setup is shown in Fig. 4. A pulse from a Ti:sapphire laser oscillator (the center wavelength, the pulse width, and the repetition rate of the laser were 800 nm, 50 fs, and 78 MHz, respectively) was inputted into the PCF. A pair of Brewster-cut BK7 prisms was used to compensate for the dispersion of the objective and to apply the chirp for the PCF. When the insertion length was set to be d as shown in Fig. 4, the value of the group delay dispersion (GDD) was $4\beta_2 d \tan 33.5°$, where $\beta_2 = 44.7$ fs^2/mm is the GVD of BK7 at 800 nm. The chirp factor C due to this GDD was given by $C = \beta_2 d / T_0^2$. Due to this chirp, the pulse width was increased by a factor of $\sqrt{1+C^2}$ (Agrawal, 2007) and the peak power P_0 of the pulse was reduced by the same factor since the pulse energy was kept constant. Thus, the electric field envelope of the pulse may be written as a Gaussian form to be $A(T) = \sqrt{P_0} e^{-(1+iC)T^2/(2T_0^2)}$, where $T_0 = 50/1.665$ fs and this functional form was used in the calculations using Eq. 4 later in this subsection.

In the first experiment, PCFs (NKT Photonics NL-1.5-670) with three different lengths (62, 114, and 166 mm) were used. The center wavelength of a fundamental soliton pulse versus an input pulse power is shown in Fig. 5 (a) and compared with the center wavelength versus an input pulse chirp shown in Fig. 5 (b). Also, the delay time versus the center wavelength of a fundamental soliton pulse is shown in Fig. 5 (c). As shown in this figure, the center wavelength of a fundamental soliton pulse changes quadratically when a fiber length was 62 mm. Similar results are obtained for 114 mm and 166 mm, although some discrepancies are noted. From Fig. 5 (c), it is seen that for the same PCF length, the delay time is independent on the control method and its dependence on wavelength is linear. Also it is shown that the delay time decreases as the fiber length becomes shorter. In the second experiment, a

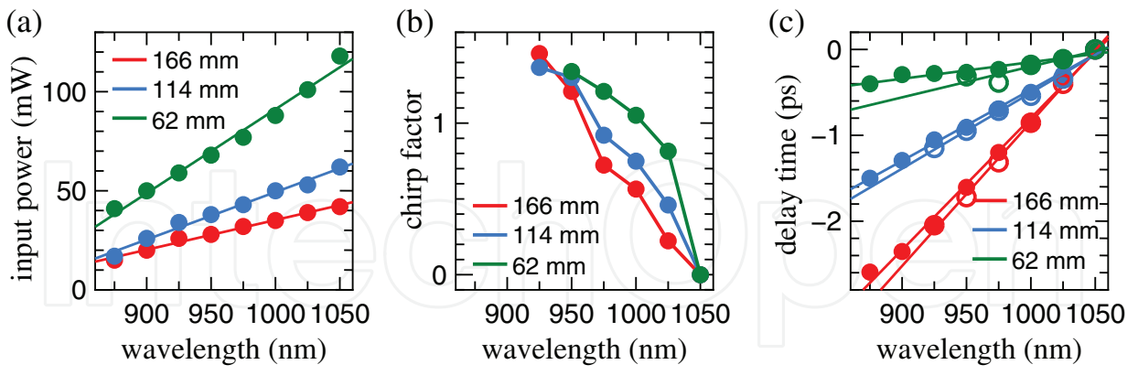

Fig. 5. Wavelength versus input power (a), wavelength versus chirp factor (b), and wavelength verses delay time (c) of soliton pulses for PCFs with different lengths.

166-mm-long PCF (NKT Photonics NL-1.5-670) whose calculated dispersion is shown in Fig. 1 (b) was used, and the results from experiment and calculations were compared. In Fig. 6 (a), experimental spectrum at 40 mW input average power is shown. There are two peaks at wavelengths near 860 nm and near 1030 nm and these correspond to fundamental soliton pulses created by the fission of an input pulse. The peak near 450 nm is a dispersive wave emitted by fundamental soliton pulses. In Fig. 6 (b), calculated spectrum at 5.74 kW input

peak power, 50 fs pulse width, and $C = 0$ is shown. The experimental and calculated spectra agreed very well as shown in this figure. The temporal waveform (Fig. 6 (c)) shows two fundamental soliton pulses at ∼0.9 ps and at ∼3.6 ps. In Fig. 7, the experimental variation of the spectral peak positions of fundamental soliton pulses is shown for different prism position d. As shown in this figure, the peak position of the fundamental soliton pulse at longest wavelength changed about 70 nm according to d. In Fig. 6, the calculated spectral and temporal intensities are shown for different chirp C calculated from d in Fig. 4. The pulse energy in these calculations was set to be 0.287 nJ, which corresponded to 5.74 kW peak power at $C = 0$. The calculated spectra showed the almost identical variation of peak positions compared with experiment. As the absolute value of C was increased, the temporal position of the most intense fundamental soliton pulse became smaller and the corresponding spectral peak wavelength became shorter. It means that as the absolute value of C was increased, the timing of the fission of an input pulse was delayed more and as a result of this, the fundamental soliton pulses experienced less soliton self-frequency shifts and less delay times at the output end of the PCF.

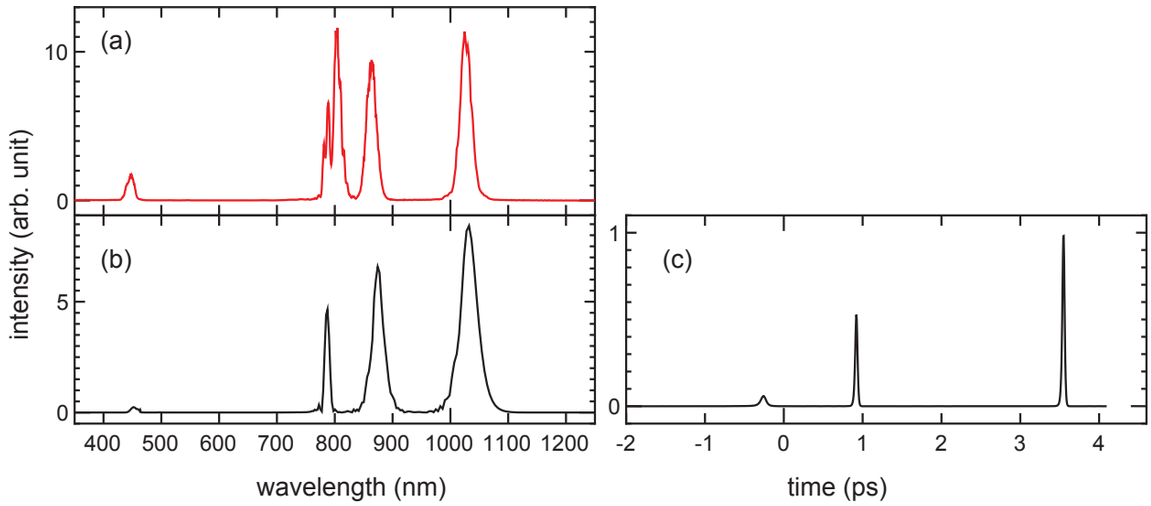

Fig. 6. (a) Experimental spectrum at 40 mW input power. Calculated spectral intensity (b) and temporal intensity (c) when a pulse with 5.74 kW peak power is inputted into a PCF.

4. Solitons for coherent anti-Stokes Raman scattering spectroscopy

Coherent anti-Stokes Raman scattering (CARS) microscopic spectroscopy is one of the nonlinear optical spectroscopy that has attracted attention recently (Cheng & Xie, 2004; Müller & Zumbusch, 2007). In CARS spectroscopy, a pump pulse (angular frequency ω_p) and a Stokes pulse (angular frequency ω_s) are used to illuminate a sample to generate an anti-Stokes signal (angular frequency $2\omega_p - \omega_s$). This signal is enhanced when the frequency difference between the pump and the Stokes pulses ($\omega_p - \omega_s$) coincides one of the Raman active vibration frequencies of the sample. The CARS signal is coherent and its intensity is much higher than that of a spontaneous Raman signal. Also, CARS signals from a fluorescent sample can be detected because the frequencies of CARS signals are higher than the frequencies of fluorescent signals. When CARS signals are detected in a microscope, the spatial resolution is expected to be high because the CARS signals are generated due to third-order nonlinear optical processes. The spectral resolution of a CARS signal is usually

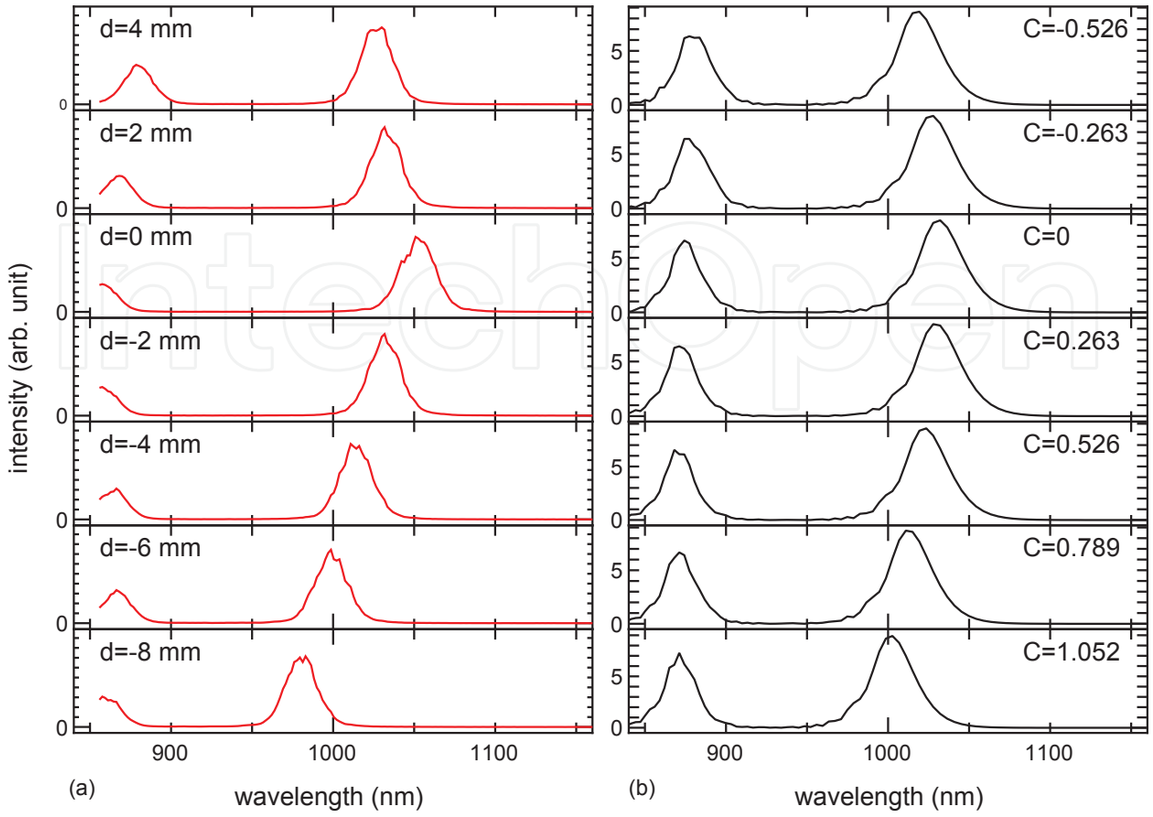

Fig. 7. (a) Experimental spectra for different prism position d. (b) Calculated spectral intensities at 0.287 nJ input pulse energy. The chirp C calculated from the position d is indicated.

determined by the spectral bandwidth of a pump pulse and its observable range is determined by the spectral bandwidth of a Stokes pulse. In multiplex CARS spectroscopy, a broadband Stokes pulse is used to detect multiple Raman vibration frequencies of a sample. To generate a broadband optical pulse, a PCF can be used and only a single laser oscillator is required to observe a broadband CARS signal by the use of a PCF. The use of a PCF to generate broadband Stokes pulses was reported in 2003 (Paulsen et al., 2003) and since then, the extent of vibration frequencies has been extended (Kano & Hamaguchi, 2005; Kee & Cicerone, 2004). However, it is difficult to generate broadband pulses with uniform spectral intensities. Also the group delays of various spectral components in a broadband pulse differ due to the dispersion property of a PCF, and thus it is difficult to generate intense broadband CARS signals. On the other hand, as shown in previous sections, the center wavelength of a soliton pulse from a PCF can be controlled easily by the power or the chirp of an input pulse, and the delay times are well known, thus it is very suitable for use in broadband or multiplex CARS spectroscopy as Stokes pluses. In this section, we show various approaches using soliton pulses for broadband CARS spectroscopy. Since the typical spectral bandwidth of a single fundamental soliton from a PCF is about 20 nm, it is necessary to change the center wavelength for broadband CARS spectroscopy. When the center wavelength is changed, the delay time changes also, so it is necessary to control the delay time at the same time. We have controlled these parameters using a pulse shaper (subsection 4.1). The other approach is to change the center wavelength of a soliton continuously by an acousto-optical modulator

(AOM) to generate quasi-supercontinuum (quasi-SC) (subsection 4.2). Also, we show results using soliton pulses for single-beam CARS spectroscopy (subsection 4.3).

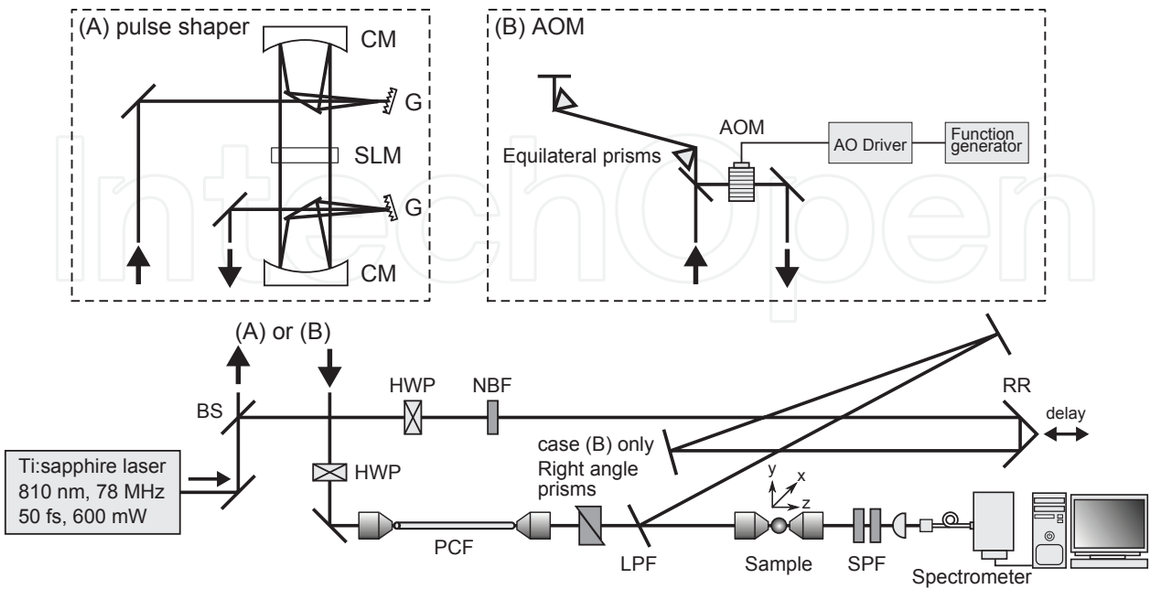

Fig. 8. Experimental setup for broadband CARS spectroscopy using a pulse shaper (A) and an AOM (B). Here, BS: beam splitter, RR: retroreflector, CM: concave mirror, G: grating, HWP: half-wave plate, NBF: narrow bandpass filter, SPF: short-wavelength pass filter, and LPF: long-wavelength pass filter.

4.1 Broadband CARS spectroscopy using a pulse shaper

Experimental setup of CARS spectroscopy using a pulse shaper is shown in Fig. 8 (A) (Tada & Karasawa, 2008; 2009). A pulse from a Ti:sapphire laser oscillator (center wavelength 810 nm, pulse width 50 fs, and repetition rate 78 MHz) was split into two pulses by a beam splitter and one of the pulse was used as a pump pulse after its spectrum was narrowed by a band pass filter (center wavelength 808 nm with a 3-nm full width at half maximum bandwidth). The other pulse was used as a Stokes pulse after it was shaped by a pulse shaper and was propagated in a 123-mm-long PCF (NKT Photonics NL-1.5-590) to generate a fundamental soliton pulse. A long-pass filter was used to eliminate the shorter-wavelength components than soliton's wavelength. Both pulses were overlapped collinearly and focused on a sample using an objective (100×, 0.5 numerical aperture). The average input powers on a sample were about 9 mW for a pump beam and about 4 mW for a Stokes beam. The signal from the sample was collected by an objective and was detected by a spectrometer (Solar TII MS-3504) with a CCD detector (Andor DV420-OE) after the spectral components of both pump and Stokes pulses were removed by the use of short-pass filters. Initially, the center wavelength of a soliton pulse from a PCF was set to be 1050 nm (which corresponds to vibration frequency $\sim$3000 cm^{-1}) by adjusting the power of an input pulse. The center wavelength of a soliton pulse was shifted to shorter wavelength by applying a phase pattern by a spatial light modulator (SLM; JenOptik SLM-S320) in a pulse shaper. The pulse shaper consists of an SLM, two pairs of gratings, concave mirrors, and folding mirrors. In the first experiment (Tada & Karasawa, 2008), six different phase patterns were used such that the

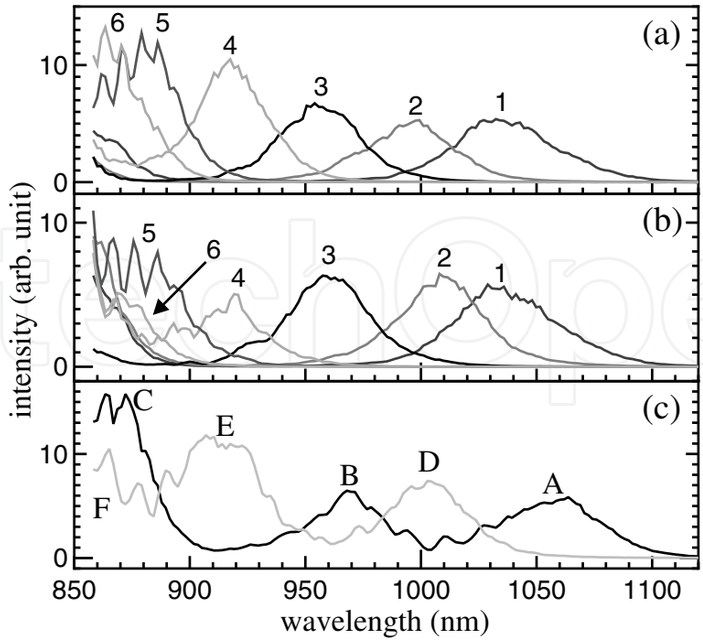

Fig. 9. Spectra of soliton pulses obtained by a pulse shaper using quadratic (a), cosine (b), and pulse train (c) phase patterns. In (c), A–F correspond to soliton pulses generated by pulses A–F in pulse trains shown in Fig. 10.

spectra of soliton pulses covered the wavelength between 850 and 1050 nm uniformly. Two different functional forms of phase patterns for varying the center wavelength of a soliton pulse were tried. One was the quadratic phase pattern of a form $(\beta_0^{(2)}/2)(\omega-\omega_0)^2$, where ω_0 was the center angular frequency of an input pulse ($\omega_0 = (2\pi c)/(800\text{ nm})$) and $\beta_0^{(2)}$ determined the chirp of an input pulse. The other was the cosine phase pattern of a form $A\cos\omega T$. When the cosine phase pattern was used, the pulse train of an original pulse was created with a period T and the peak amplitude of the central pulse was determined by the Bessel function of zero order $J_0(A)$ (Morita & Toda, 2005). The period T was set to be 500 fs in experiment such that the timing of only the central pulse in a pulse train matched with a pump pulse. In both cases, the phase pattern of a form $\beta_0^{(1)}(\omega-\omega_0)$ was added to control the delay time of an input pulse with respect to a pump pulse, where $\beta_0^{(1)}$ is a group delay. Moreover, the phase pattern of a form $(\beta_{00}^{(2)}/2)(\omega-\omega_0)^2$ with $\beta_{00}^{(2)} = -200\text{ fs}^2$ was added for all phase patterns to compensate for the dispersion of an objective lens in front of a PCF. To adjust the delay time of a soliton pulse with a pump pulse, the group delay $(\beta_0^{(1)})$ of an input pulse was set to be different for a soliton pulse with a different center wavelength. In Fig. 9, the spectra of soliton pulses with six different center wavelengths are shown for both the quadratic (a) and the cosine (b) phase patterns. As shown in this figure, by using six soliton pulses with different center wavelengths, the spectral regions between 850 and 1050 nm were covered almost uniformly. The exposure time to obtain CARS signals was set to be one second for each soliton pulse with a different wavelength, thus the total exposure time to obtain CARS signals between 500 and 3100 cm^{-1} was six seconds. In addition to this, the switching time of the phase pattern in a SLM was required (about 0.3 second for every switching). In the later

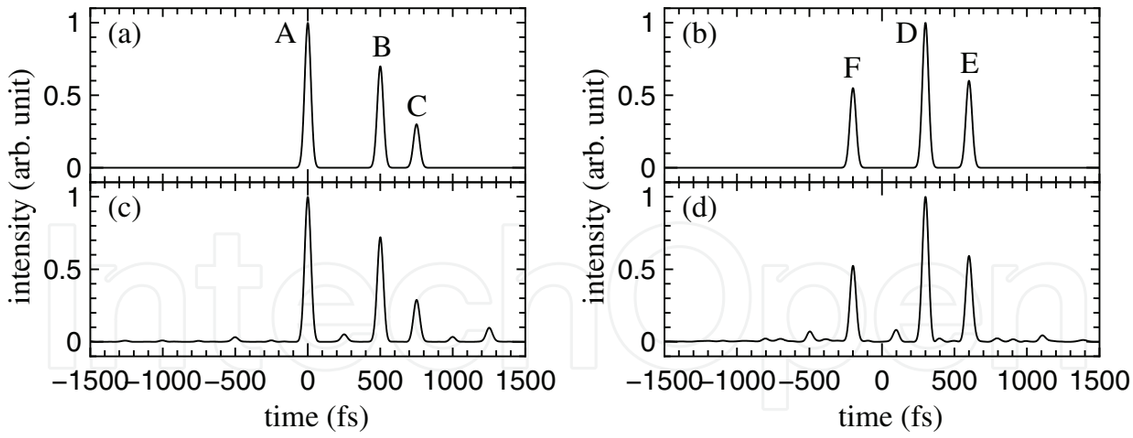

Fig. 10. Target pulse waveforms ((a) and (b)) for generating pulse train phase patterns and the optimized waveforms ((c) and (d)).

experiment (Tada & Karasawa, 2009), pulse trains were created to generate multiple solitons with different center wavelengths by a single phase pattern. Here, we prepared two different phase patterns for the SLM to generate the five fundamental soliton pulses. We adjusted the power ratios of pulses in a pulse train for varying the wavelengths of soliton pulses. Also, we adjusted the temporal delays of pulses in a pulse train such that all fundamental pulses arrived the sample at the same time. In Fig. 10, the two target pulse waveforms used in experiment for generating fundamental soliton pulses are shown. In a target pulse train 1 (Fig. 10 (a)), there were three pulses A (power ratio 1, delay time 0 fs), B (power ratio 0.7, delay time 500 fs), and C (power ratio 0.3, delay time 750 fs) for generating soliton pulses. In a target pulse train 2 (Fig. 10 (b)), there were two pulses D (power ratio 1.0, delay time 300 fs) and E (power ratio 0.6, delay time 600 fs). The pulse F (power ratio 0.55, delay -200 fs) was added in the pulse train for adjusting the total power of the pulse train 2 with respect to the pulse train 1. Since this pulse was not used in CARS spectroscopy, its delay time was shifted intentionally such that it did not arrive the sample at the same time with other pulses. All pulses in pulse trains were assumed to be Gaussian pulses with the full width at half maximum pulse widths to be 50 fs. The phase patterns for the SLM to generate these target pulses were created using genetic algorithms (Goldberg, 1989), where each phase pattern was optimized such that the difference between the shaped pulse obtained numerically and the target pulse became minimum. Here, the shaped pulse was calculated numerically by the inverse Fourier transform of the input pulse spectrum after its phase was modified according to the phase pattern, where the input pulse was assumed to be a 50-fs Gaussian pulse. The pulse waveforms obtained numerically after their phase patterns were optimized by the genetic algorithms are shown in Fig. 10 (c) and (d). As shown in Fig. 10, these numerically-obtained pulses using the optimized phase patterns agreed well with target pulses. The spectra of soliton pulses after these pulse trains were propagated in a PCF are shown in Fig. 9 (c). In this figure, two measured spectra with different phase patterns are shown and spectral peaks A–F corresponded to soliton pulses generated by pulses A–F in Fig. 10. As shown in this figure, the wavelength range between 860 and 1070 nm was covered by five fundamental soliton pulses. As mentioned above, the spectral peak F did not affect CARS measurements since its temporal timing was shifted. By switching these two phase patterns in the SLM, it was possible to measure broadband CARS signals automatically. The exposure time for each phase pattern was set to be 1 s and the additional time 0.4 s was required for switching the phase pattern in the SLM. Thus, the total

measurement time was 2.4 s. The results of CARS spectroscopy of a polystyrene (PS) sample

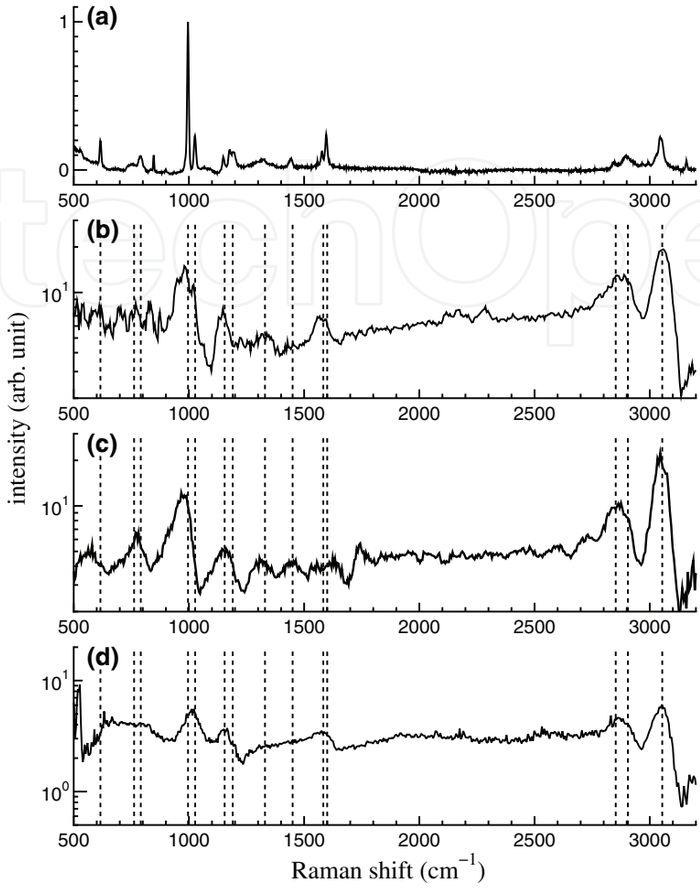

Fig. 11. Spontaneous Raman spectrum (a) and CARS spectra using a pulse shaper with a quadratic (b), cosine (c), and pulse train (d) phase patterns of a 6-μm diameter polystyrene bead sample. In (b)–(d), peak positions of spontaneous Raman spectrum are shown by dashed lines.

are shown and compared with the result of spontaneous Raman spectroscopy in Fig. 11. In this figure, the CARS signal from a sample was normalized by the signal from a glass substrate to show the resonant contribution of CARS signal clearly (Kee & Cicerone, 2004). All results using a pulse shaper (quadratic, cosine, and pulse train phase patterns) agreed well and the Raman peaks observed by spontaneous Raman spectroscopy were observed clearly in CARS signals between 500 and 3100 cm^{-1}. The spectral widths of Raman peaks were determined by the spectral width of a pump pulse and in our setup, the spectral resolution was about 50 cm^{-1}. The exposure time for the method using phase patterns for pulse trains was 2.4 s and is less than half compared with the methods using phase patterns for single soliton pulses. It was because the effective bandwidth of the Stokes pulse was multiplied by a number of pulses in a pulse train. Here, we have limited the number of pulses in a pulse train to be three due to the constraint of the available power from a laser, but it is straightforward to increase the number if enough power is available. It is demonstrated that the broadband fundamental soliton pulses can be generated by a pulse shaper and are very useful for CARS spectroscopy.

4.2 Quasi-supercontinuum broadband CARS spectroscopy using an acousto-optical modulator

Since the center wavelength of a soliton pulse can be changed by varying the input pulse power of a PCF, it is possible to generate pulse trains whose center wavelengths change continuously by modulating the input power rapidly. In this way, quasi-supercontinuum (quasi-SC) in the wavelength range from 1.56 to 1.9 μm was generated using soliton pulses from a highly nonlinear fiber by scanning the input power by an acousto-optical modulator (AOM) and its application to optical coherence tomography (OCT) was mentioned (Sumimura et al., 2008). In OCT, the adjustment of the group delays between different spectral components is not necessary since the shape of the interference signal depends on the spectrum of the light source only. On the other hand, the adjustment is very important in CARS spectroscopy to obtain strong broadband CARS signals. In this study, we have generated quasi-SC in the wavelength range from 0.85 to 1.1 μm using a PCF and applied to CARS spectroscopy, where the power modulation was performed by an AOM and the group delay adjustment was performed by simply placing a pair of prisms after the PCF, since the group delay of the soliton pulses depended on wavelength approximately linearly as mentioned in Chapter 3.

Experimental setup for quasi-SC CARS spectroscopy s shown in Fig. 8 (B) (Tada & Karasawa, 2010). A pulse from a Ti:sapphire laser oscillator (center wavelength 810 nm, pulse width 50 fs, and repetition rate 78 MHz) was split into two pulses by a beam splitter and one of the pulse was used as a pump pulse after its spectrum was narrowed by a band pass filter (center wavelength 808 nm with a 3-nm full width at half maximum bandwidth). The other pulse was used as a Stokes pulse after its power was modulated by an AOM (ISOMET M1137-SF-40L-1.5) and was propagated in a 120-mm-long PCF (NKT Photonics NL-1.5-590) to generate quasi-SC, where a pair of SFL11 equilateral prisms was used to compensate for the dispersion of the AOM. For the modulation of the AOM, a 100-kHz sinusoidal wave was used. A long-pass filter (cut-off wavelength 840 nm) was used to eliminate the shorter-wavelength components than the wavelengths of solitons. A pair of SFL11 right angle prisms was used to adjust the group delays of soliton pulses with different center wavelengths.

Both pump and Stokes pulses were overlapped collinearly and focused on a single 6-μm-diameter polystyrene bead sample using an objective (100×, 0.9 numerical aperture). The CARS signal from the sample was collected by an objective and was detected by a spectrometer (Solar TII MS-3504) with a CCD detector (Andor DV420-OE) after the spectral components of both pump and Stokes pulses were removed by the use of short-pass filters (cutoff wavelengths 785 and 850 nm). The exposure time for taking a CARS spectrum was two second. In Fig. 12 (a), the spectrum of generated quasi-SC when an AOM was modulated by a 100-kHz sinusoidal wave is shown. As shown in this figure, broadband quasi-SC, which had a sufficient spectral intensity for the CARS spectroscopy in the wavelength range from 850 to 1100 nm, was generated, which corresponded to CARS wave number between 500 and 3100 cm^{-1}. In Fig. 12 (b), the normalized CARS spectrum of a single 6-μm-diameter polystyrene bead sample using quasi-SC are shown and it is compared with the known spontaneous Raman peaks. As shown in this figure, most spectral peaks of the polystyrene sample were observed clearly between 900 and 3100 cm^{-1}. The exposure time of 2 s was shorter than the exposure time in the previous subsection (2.4 s) using the same spectrometer for the measurement with the similar signal to noise ratio. It is demonstrated that the quasi-SC is very useful for broadband CARS spectroscopy.

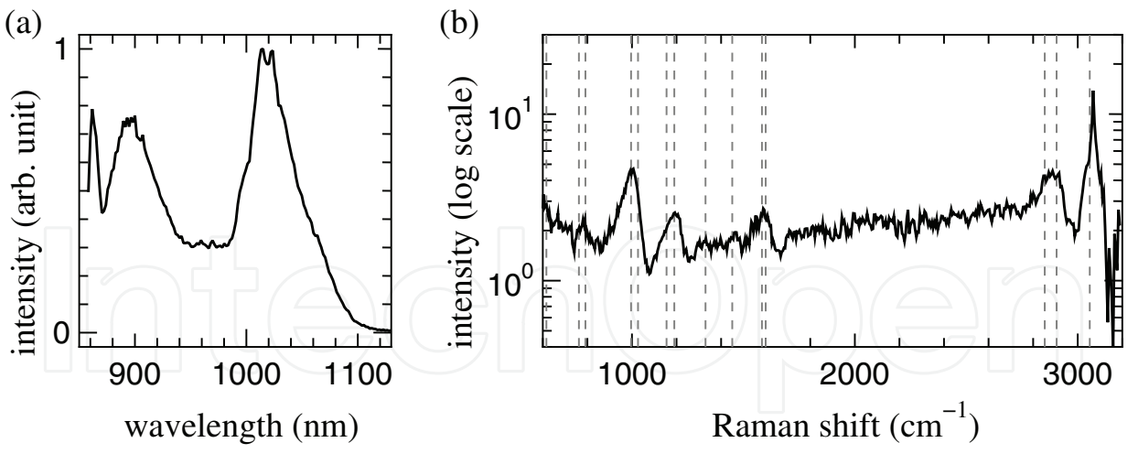

Fig. 12. (a) The spectrum of quasi-SC. (b) The normalized CARS spectrum using quasi-SC of a 6-μm diameter polystyrene bead sample. Peak positions of spontaneous Raman spectrum are shown by dashed lines.

4.3 Single-beam CARS spectroscopy

As shown in previous subsections, two separate beams, a pump beam and a Stokes beam, have to be collinearly overlapped and focused on a sample using an objective lens in CARS spectroscopy in general. However, the adjustments of these two beams, necessary to generate strong CARS signals, are sometimes difficult. Therefore, it is desirable to perform CARS spectroscopy using a single beam. It is necessary to generate a single beam that contains both pump and Stokes spectral components to perform single-beam CARS spectroscopy. In

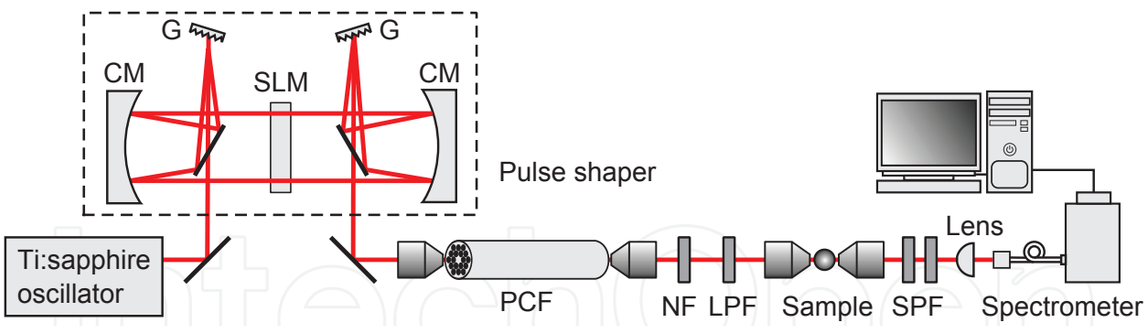

Fig. 13. Experimental setup for single-beam CARS spectroscopy. Here, NF: notch filter, LPF: long-wavelength pass filter, SPF: short-wavelength pass filter, G: grating, and CM: concave mirror.

our setup (Tada & Karasawa, 2011), two pulses, one for generating a wavelength-tunable fundamental soliton pulse and the other for generating a narrowband pump pulse, are shaped by a pulse shaper and inputted into a PCF. The fundamental soliton Stokes pulse is generated by redshifting the input pulse spectrum through the soliton self-frequency shift in a PCF and the amount of this shift is controlled by the power of an input pulse. The pulse for a pump pulse is negatively chirped by a pulse shaper for the spectral compression in a PCF

(Andresen et al., 2005), which is important for obtaining a narrowband pump pulse to achieve a high spectral resolution while retaining most of the pulse energy.

The experimental setup of single-beam CARS spectroscopy is shown in Fig. 13. Two pulses with different intensities were shaped from a single pulse from a Ti:sapphire laser oscillator (the center wavelength 797 nm, the pulse width 50 fs, the average power 570 mW, and the repetition rate 78 MHz) and propagated in a 119-mm-long and 1.5-μm-core-diameter PCF (NKT Photonics NL-1.5-590). An input pulse with a negative chirp was compressed spectrally due to the self-phase modulation until it became almost transform-limited. The amount of chirp, the input power, and the fiber length were adjusted to obtain an optimal spectral compression. In Fig. 14, the target pulse waveforms used in the experiment for generating

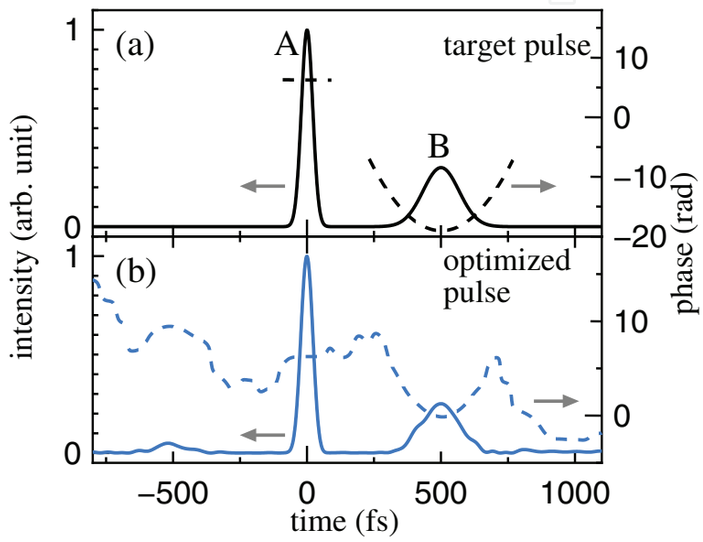

Fig. 14. (a) The intensity and the phase of a target pulse for single-beam CARS spectroscopy, where pulse A is for generating a soliton pulse and pulse B is for generating a narrowband pump pulse. (b) The intensity and the phase of an optimized pulse.

two pulses are shown by black curves. In a target pulse, there were two pulses, namely, pulse A (power ratio 1 and delay time 0 fs) for generating a Stokes soliton pulse and pulse B (power ratio 0.3 and delay time 500 fs). Pulse B was negatively chirped for spectral compression to generate a narrowband pump pulse (chirp factor -3). The phase pattern for generating these pulses were optimized by the genetic algorithms (Goldberg, 1989). By adjusting the relative delay time between these two input pulses for a PCF, it was possible to generate a single beam that contained timing-matched pump and Stokes pulses at the sample position. To determine the delay time between two pulses, a β-BaB_2O_4 (BBO) crystal was set at the sample position and the sum-frequency signals of the pump and Stokes pulses were measured. Long-pass filters (cutoff wavelengths 793 and 590 nm) and a notch filter (center wavelength 825 nm and bandwidth 40 nm) were used to limit the bandwidth of the spectrally compressed pump pulse and remove the wavelengths shorter than the pump pulse. CARS signals were generated by the output beam from a PCF, where the beam was tightly focused on a sample by an objective lens (100$\times$ and 0.9 numerical aperture). The generated CARS signals from the sample were collected by a microscope objective lens (100$\times$ and 0.7 numerical aperture), where the spectral components at the pump and longer wavelengths were removed by the

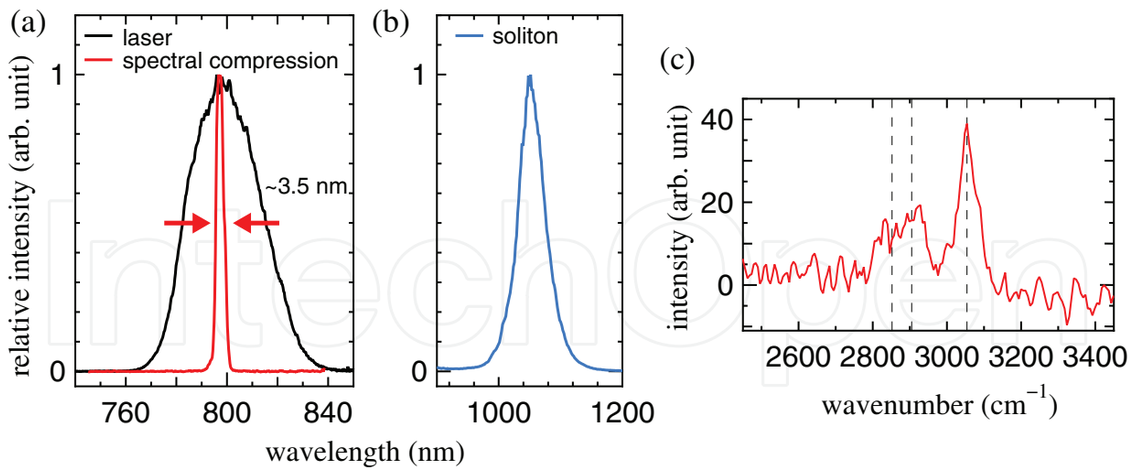

Fig. 15. In (a), the spectra from laser and a narrowband pump pulse are shown. In (b), the spectrum of a soliton pulse is shown. In (c), the CARS signal of a 6-μm-diameter polystyrene bead sample is shown, where known Raman peak positions are shown by dashed lines.

combination of short-pass filters (cutoff wavelengths 785 and 850 nm). The CARS signals from the sample were detected by a spectrometer (Solar TII MS-3504) with a CCD detector without an intensifier (Andor DV420-OE). The exposure time for taking a CARS spectrum was 5 s.

Figure 15 (a) and (b) show the spectra of the output beam from a PCF after notch and long-pass filters when a pulse with about 88 mW average power was inputted into the PCF. In Fig. 15 (a), a black curve shows the spectrum of a laser pulse with a full width at half maximum (FWHM) of about 32 nm. A red curve shows the spectrum of a pump pulse after the PCF and the combinations of filters with a width of about 3.5 nm, which was about 11% of the original bandwidth. The spectral resolution using this pump pulse was about 55 cm^{-1}. A Stokes pulse shown in Fig. 15 (b) was generated from a PCF as a fundamental soliton pulse at the center wavelength 1052 nm, which was tuned to match the Raman shift of about 3000 cm^{-1}. When the input average power for the PCF was 88 mW, the output average power was 26 mW and the average powers of the beam after a long-pass filter for pump and Stokes components were 2 and 3 mW, respectively. Figure 15 (c) shows the CARS signals generated from a single 6-μm-diameter polystyrene bead. As shown in this figure, the CARS signals of the polystyrene were observed from 2800 to 3100 cm^{-1} that corresponded to well-known C-H stretching vibration modes (the Raman shifts for symmetric aliphatic 2852 cm^{-1}, asymmetric aliphatic 2905 cm^{-1}, and aromatic 3054 cm^{-1} are shown in Fig. 15 (c) by vertical lines).

It is demonstrated that CARS spectroscopy can be performed using a single-beam setup with a pulse shaper and a fundamental soliton pulse from a PCF. Unlike previous single-beam CARS setups using a pulse shaper, this setup can be used to observe CARS signals from 2800 to 3100 cm^{-1}. The spectral resolution of the setup was determined by the bandwidth of the combinations of notch and bandpass filters. Since the wavelength of the soliton Stokes pulse can be varied by adjusting the input power, it is straightforward to perform broadband CARS measurements using this setup.

5. Solitons for optical coherence tomography

Optical coherence tomography (OCT) is a technique that images the internal structure of biological or medical samples noninvasively and nondestructively by using a low-coherent light source and a Michelson interferometer. OCT was developed in the early 1990s (Huang et al., 1991). The depth resolution of the OCT is determined by the spectral width of the light source. Thus it is important to broaden the spectral width of the light source for improving the resolution of OCT. Also it is important to make the spectral shape of the light source simple, e.g. the Gaussian shape, since in that case, the side pulses of an interference signal, which become noises in an OCT image, become small. The depth resolution of the OCT is determined by the coherence length l_c, which is the FWHM width of the interference signal and it is given by $l_c = a\lambda_0^2/\Delta\lambda$ for the intensity spectrum with the center wavelength λ_0 and the FWHM bandwidth $\Delta\lambda$. a is a constant and $a = 0.44$ for a Gaussian spectrum and $a = 0.39$ for a sech^2 spectrum. Supercontinuum from a PCF was used to improve the resolution of OCT (Hartl et al., 2001). However, since there are many peaks in the spectrum of the supercontinuum light from a PCF, there are many side pulses in the interference signal and these become noises in an OCT image. As shown in previous sections, the fundamental soliton pulses from a PCF ranges in a wavelength region between 0.85 μm and 1.05 μm when a Ti:sapphire laser is propagated and the spectral shapes of them are simple. Also, since the penetration depth of 1.0-1.3 μm light is maximum and the attenuation due to absorption and scattering is minimum in biological samples (Lim et al., 2005), it is beneficial to use a light source in this wavelength region. The center wavelength of the fundamental soliton pulse shifts to longer wavelength as it propagates in a PCF and it can be controlled by changing the power of an input pulse. When the power of an input pulse is changed continuously, the wavelength of a soliton pulse changes continuously and the soliton pulse can be used as a quasi-supercontinuum (quasi-SC) light source and its use in OCT as a light source has been studied (Sumimura et al., 2008) in wavelength $\sim$1.5 μm. Here, we show results using a pulse train generated by a pulse shaper and quasi-SC in the wavelength range between 900 and 1000 nm generated by an AOM.

5.1 Pulse train OCT using a pulse shaper

The experimental setup is shown in Fig. 16 (A) (Takabatake et al., 2010). The pulse emitted from a Ti:sapphire laser (pulse width 50 fs, center wavelength 810 nm, repetition rate 78 MHz, average power 600 mW) was transformed into a pulse train with three pulses by a pulse shaper, where the interval times and the peak power ratios between pulses were controlled as in CARS experiment (subsection 4.1). These parameters were optimized to obtain the best interference signal in OCT. The pulse train was propagated in a 45 cm PCF (NKT Photonics NL-1.5-670) and the pulse train which had overlapped spectra of each fundamental soliton pulse was generated. The input power of a PCF was adjusted to be 123 mW and the power of a single soliton pulse generated was 3 mW. The polarization direction of the input pulse train was optimized by a half wavelength plate to maximize the output power from the PCF. Also, a polarization plate was used to select the polarization direction of an output beam from the PCF. A long-pass filter with 840-nm cut-off wavelength was used to transmit only soliton pulses. The spectrum of a soliton pulse train was measured by a spectrometer and an interference signal was measured by a Michelson interferometer with a balanced photo detector. In the experiment, a mirror was placed at a sample position to obtain an interference signal and to evaluate its width. The position of a reference mirror was varied by a piezo stage

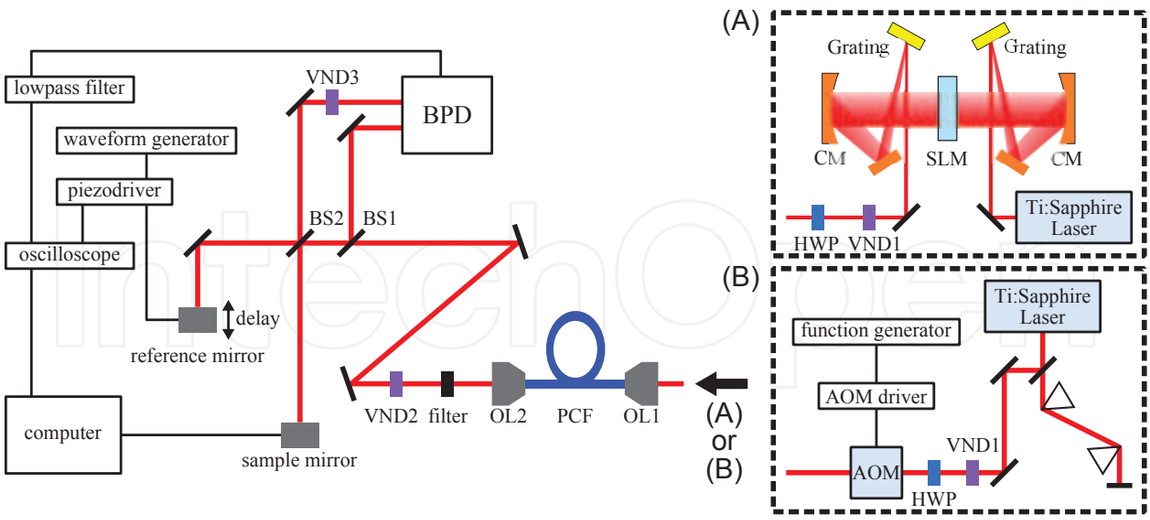

Fig. 16. Experimental setup for the soliton-based OCT using a pulse shaper (A) and an AOM (B). Here, VND: variable neutral density filter, CM: concave mirror, HWP: half-wave plate, OL: objective lens, BPD: balanced photo detector, and BS: beam splitter.

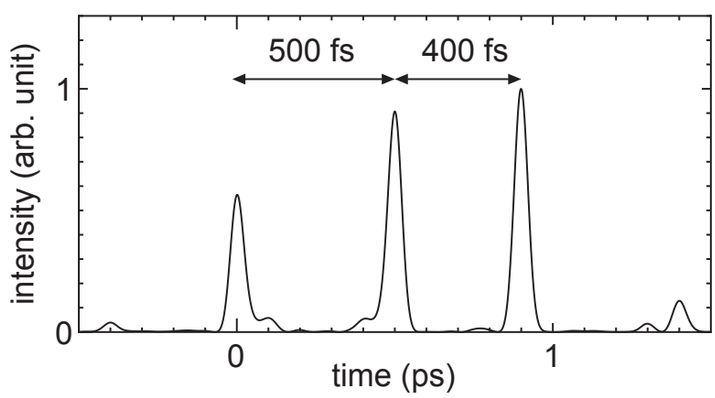

Fig. 17. Pulse waveforms for generating a pulse train of three soliton pulses obtained after optimized by a genetic algorithm.

and the modulation frequency of the delay was set to be 0.5 Hz. In experiment using a pulse shaper, a pulse train of three pulses was created, where the interval times and the power ratios of three pulses were set to be 500 fs and 400 fs, and 1.0:1.25:1.33 respectively after optimization. Since the soliton created by a pulse with a larger peak power delayed more in a fiber, it was necessary to input a pulse with a larger peak power later into a fiber to avoid overlapping with other soliton pulses. The phase pattern for generating the pulse train was optimized by a genetic algorithm (Goldberg, 1989). In Fig. 17, the temporal waveform of the pulse train, where the optimized phase pattern was used, is shown. In Fig. 18, the interference signal and the spectrum obtained by the pulse train (three soliton pulses) are compared with results without using a pulse train (a single soliton pulse). The spectral width ($\Delta\lambda$) of the single soliton was 21.4 nm and it became 64.0 nm when the pulse train was used. The coherence length (l_c) of the single soliton was 17.6 μm and it became 8.3 μm for the pulse train. From this result, it is demonstrated that the resolution of OCT can be improved by superimposing

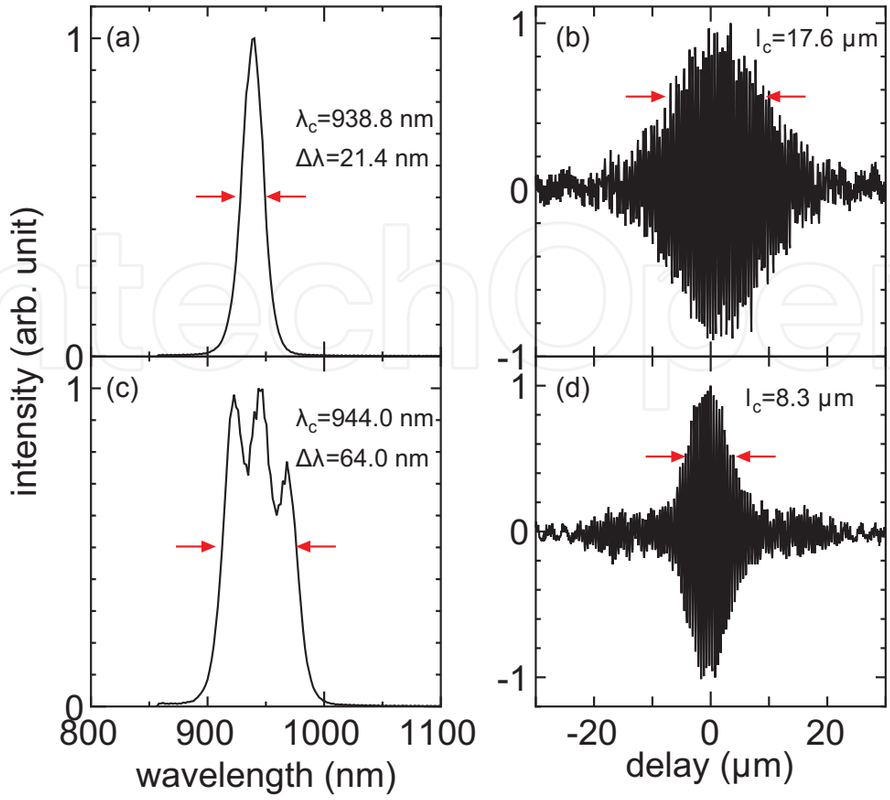

Fig. 18. The spectrum (a) and the interference signal (b) of a single soliton pulse compared with the spectrum (c) and the interference signal (d) of a pulse train composed of three soliton pulses.

soliton pulses using a pulse train. In this case, only three soliton pulses were used due to the constraint of the available power for the input power of a PCF. A pulse train that contains more pulses with the broader spectrum may be obtained if more input power is available.

5.2 Quasi-SC OCT using an acousto-optical modulator

In this experiment, a pulse shaper was replaced by an AOM and a prism pair for dispersion compensation for the AOM, as shown in Fig. 16 (B). The AOM was driven either by a sinusoidal wave or a triangle wave for modulating the input power of a PCF. The modulation frequency was set to be 5 KHz. By inputting modulated pulses (average power 64 mW) into a PCF, quasi-SC were generated, since the center wavelength of a soliton pulse changed according to the input power of a PCF due to the soliton self-frequency shift. The spectra of these quasi-SC were considered to be broadened if the measurement time was much longer than the modulation period of the AOM (0.2 ms in this case). In Fig. 19, the interference signals and the quasi-SC spectra are shown. The spectral widths ($\Delta\lambda$) of the quasi-SC for a sinusoidal wave modulation and a triangle wave modulation were 113.3 and 102.4 nm, where the exposure time of a spectrometer was 50 ms. The coherence length (l_c) of these quasi-SC were 6.1 and 6.5 μm, which are about one-third of the coherence length of a single soliton pulse shown in Fig. 18 (b). The quasi-SC spectrum obtained using a triangle wave (Fig. 19 (c)) was more uniform than the spectrum obtained using a sinusoidal wave (Fig. 19 (a)) since the

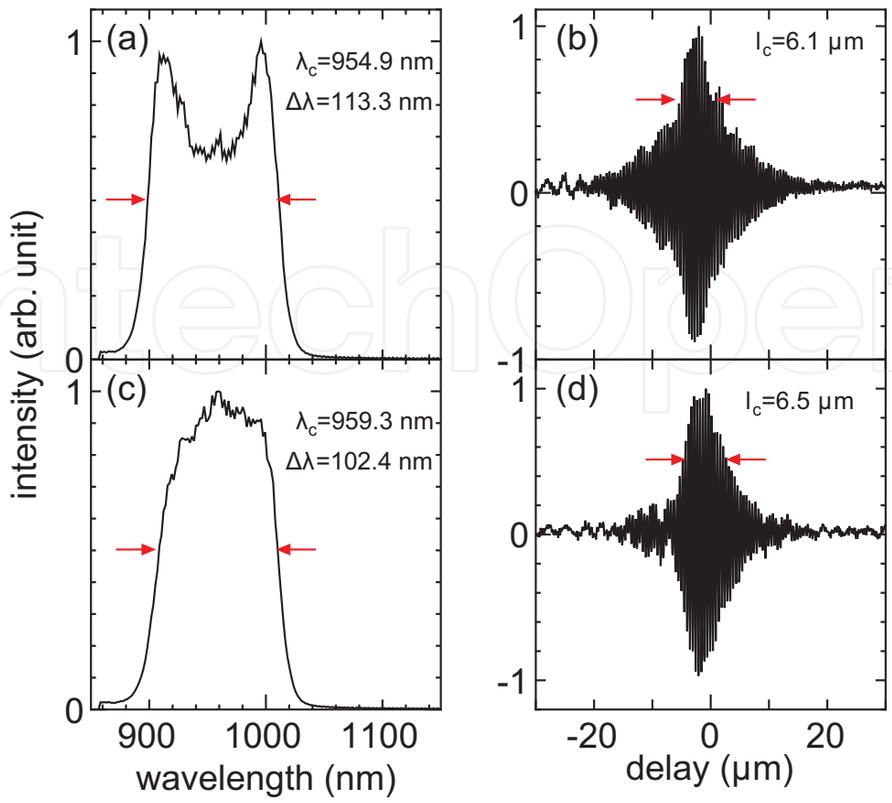

Fig. 19. The spectrum (a) and the interference signal (b) of quasi-SC using a sinusoidal wave compared with the spectrum (c) and the interference signal (d) of quasi-SC using a triangle wave.

variation of the power inputted into a PCF using a triangle wave was more uniform than that using a sinusoidal wave. From these results, it is demonstrated that the resolution of OCT can be improved by using a quasi-SC.

5.3 Comparison between methods using a pulse train and quasi-SC

By comparing the spectrum using a pulse train with three pulses shown in Fig. 18 (c) with the spectra using an AOM shown in Fig. 19 (a) and (c), we see that the spectral widths of the quasi-SC were broader than that of a pulse train and as a result, the coherent lengths of quasi-SC were smaller than that of a pulse train. Therefore it is advantageous to use quasi-SC to obtain the better resolution in OCT. This is because the throughput of an AOM was higher than that of a pulse shaper in our experimental setups. Also, it is possible to modify the spectral shape by changing the modulation waveform when using an AOM. However, the spectrum obtained using an AOM shown in Fig. 19 (a) and (c) were not stationary but the center wavelength of a soliton in the quasi-SC varied with the modulation frequency of an AOM (5 kHz). On the other hand, the spectrum obtained using a pulse train shown in Fig. 18 (c) was obtained by superimposing three soliton pulses and was stationary with the repetition rate of a laser (78 MHz). The method using quasi-SC may have a problem when the scanning speed of the OCT setup becomes comparable to the modulation speed of the AOM.

6. Conclusion

In this chapter, fundamental soliton pulses generated from a PCF were introduced and their applications in CARS spectroscopy and OCT were explained. The wavelength of the soliton pulse changes due to the self-frequency shift and it can be controlled by the power and/or the chirp of a pulse inputted into the PCF. At the same time, the delay time of the soliton pulse changes, which can be estimated relatively easily. The use of a pulse shaper is very useful to control the wavelength and the delay time simultaneously and this was used effectively in CARS spectroscopy experiment. In CARS experiment, broadband Stokes soliton pulses were generated and the broadband CARS spectroscopy setups were demonstrated. Also, a single-beam CARS spectroscopy setup was demonstrated using the fundamental soliton pulse. In OCT experiment, broadband pulses in wavelength between 900 and 1000 nm were generated using soliton pulses and the improvement of the resolution of the interference signals were demonstrated using these pulses.

7. Acknowledgements

We would like to appreciate Yoshihiko Takabatake, Minoru Bunya, Chihiro Satoh and Ryoh Shirakawa who contributed to the work presented in this book chapter. This work was supported in part by a Grant-in-Aid for Scientific Research (C) from the Japan Society for the Promotion of Science (JSPS) and a Grant-in-Aid for JSPS Fellows.

8. References

Agrawal, G. P. (2007). *Nonlinear Fiber Optics Fourth Ed.*, Elsevier, Burlington, MA, USA.

Andresen, E. R., Thøgersen, J. & Keiding, S. R. (2005). Spectral compression of femtosecond pulses in photonic crystal fibers, *Opt. Lett.* Vol. 30 pp. 2025–2027.

Blow, K. J. & Wood, D. (1989). Theoretical description of transient stimulated Raman scattering in optical fibers, *IEEE J. Quantum Electron.* Vol. 25 pp. 2665–2673.

Cheng, J. X. & Xie, X. S. (2004). Coherent anti-Stokes Raman scattering microscopy: instrumentation, theory, and applications, *J. Phys. Chem. B.* Vol. 108 pp. 827–840.

Dudley, J. M., Genty, G. & Coen, S. (2006). Supercontinuum generation in photonic crystal fiber, *Rev. Mod. Phys.* Vol. 78 pp. 1135–1184.

Goldberg, D. E. (1989). *Genetic Algorithms in Search, Optimization and Machine Learning*, Addison-Wesley, Reading, MA, USA.

Gordon, J. P. (1986). Theory of the soliton self-frequency shift, *Opt. Lett.* Vol. 11, pp. 662–664.

Hartl, I., Li, X. D., Chudoba, C., Ghanta, R. K., Ko, T. H., Fujimoto, J. G., Ranka, J. K. & Windeler, R. S. (2001). Ultrahigh-resolution optical coherence tomography using continuum generation in an air-silica microstructure optical fiber, *Opt. Lett.* Vol. 26 pp. 608–610.

Hasegawa, A. (1992). Optical solitons in fibers: theoretical review, *in* Taylor, J. R. (ed.), *Optical Solitons – Theory and Experiment* , Cambridge Univ. Press, Cambridge, pp.1–29.

Huang, D., Swanson, E. A., Lin, C. P., Schuman, J. S., Stinson, W. G., Chang, W., Hee, M. R., Flotte, T., Gregory, K., Puliafito, C. A. & Fujimoto, J. G. (1991). Optical coherence tomography, *Science* Vol. 254 pp. 1178–1181.

Husakou, A. V. & Herrmann, J. (2001). Supercontinuum generation of higher-order solitons by fission in photonic crystal fibers, *Phys. Rev. Lett.* Vol. 87 pp. 203901-1–203901-4.

Kano, H. & Hamaguchi, H. (2005). Ultrabroadband (>2500 cm^{-1}) multiplex coherent anti-Stokes Raman scattering microspectroscopy using a supercontinuum generated from a photonic crystal fiber, *Appl. Phys. Lett.* Vol. 86 pp. 121113-1–121113-3.

Karasawa, N., Nakamura, S., Nakagawa, N., Shibata, M., Morita, R., Shigekawa, H., & Yamashita, M. (2001). Comparison between theory and experiment of nonlinear propagation for a-few-cycle and ultrabroadband optical pulses in a fused-silica fiber, *IEEE J. Quantum Electron.* Vol. 37, pp. 398–404.

Karasawa, N., Tada, K., & Ohmori, H. (2007). The comparison between experiment and calculation of the chirp-controlled Raman self-frequency shift in a photonic crystal fiber, *IEEE Photon. Technol. Lett.* Vol. 19, pp. 1292–1294.

Kee, T. W. & Cicerone, M. T.. (2004). Simple approach to one-laser, broadband coherent anti-Stokes Raman scattering microscopy *Opt. Lett.* Vol. 29 pp. 2701–2703.

Lim, H., Jiang, Y., Wang, Y., Huang, Y.-C., Chen, Z. & Wise, F. W. (2005). Ultrahigh-resolution optical coherence tomography with a fiber laser source at 1 μm, *Opt. Lett.* Vol. 30, pp. 1171–1173.

Mitschke, F. M. & Mollenauer, F. (1986). Discovery of the soliton self-frequency shift, *Opt. Lett.* Vol. 11 pp. 659–661.

Morita, R. & Toda, Y. (2005). Field manipulation of ultrabroadband optical pulses, *in* Yamashita, M., Shigekawa, H. & Morita, R. eds., *Mono-Cycle Photonics and Optical Scanning Tunneling Microscopy*, Springer, Berlin, pp. 251–283.

Müller, M. & Zumbusch, A. (2007). Coherent anti-Stokes Raman scattering microscopy, *ChemPhysChem* Vol. 8 pp. 2156–2170.

Paulsen, H. N.. Hilligsøe, K. M., Thøgersen, J, Keiding, S. R. & Larsen, J. J. (2003). Coherent anti-Stokes Raman scattering microscopy with a photonic crystal fiber based light source, *Opt. Lett.* Vol. 28 pp. 1123–1125.

Ranka, J., Windeler, R. S. & Stentz, A. J. (2000). Visible continuum generation in air-silica microstructure optical fibers with anomalous dispersion at 800 nm, *Opt. Lett.* Vol. 25, pp. 25–27.

Satsuma, J. & Yajima, N. (1974). Initial value problems of one-dimensional self-modulation of nonlinear waves in dispersive media, *Suppl. Prog. Theor. Phys., Japan* Vol. 55 pp. 284–306.

Schrader, D. (1995). Explicit calculation of *N*-soliton solutions of the nonlinear Schroedinger equation, *IEEE J. Quantum Electron.* Vol. 31, pp. 2221–2225.

Sumimura, K., Ohta, T. & Nishizawa, N. (2008). Quasi-super-continuum generation using ultrahigh-speed wavelength-tunable soliton pulses, *Opt. Lett.* Vol. 33, pp. 2892–2894.

Tada, K. & Karasawa, N. (2008). Broadband coherent anti-Stokes Raman scattering spectroscopy using pulse-shaper-controlled variable-wavelength soliton pulses from a photonic crystal fiber, *Jpn. J. Appl. Phys.* Vol. 47 pp. 8825–8828.

Tada, K. & Karasawa, N. (2008). Coherent anti-Stokes Raman scattering microspectroscopy using a fundamental soliton pulse generated from a photonic crystal fiber, *in* Tanio, N. & Sasabe, H. eds., *Optical Materials and Devices New Stage*, PWC Publishing, Chitose, Japan, pp. 215–220.

Tada, K. & Karasawa, N. (2009). Broadband coherent anti-Stokes Raman scattering spectroscopy using soliton pulse trains from a photonic crystal fiber, *Opt. Commun.* Vol. 282 pp. 3948–3952.

Tada, K. & Karasawa, N. (2010). Broadband coherent anti-Stokes Raman scattering spectroscopy using a quasi-supercontinuum light source, *in Conference on Lasers and Electro-Optics*, OSA Technical Digest, paper JTuD72.

Tada, K. & Karasawa, N. (2011). Single-beam coherent anti-Stokes Raman scattering spectroscopy using both pump and soliton Stokes pulses from a photonic crystal fiber, *Appl. Phys. Express* Vol. 4 pp. 092701-1–092701-3.

Takabatake, Y., Tada, K. & Karasawa, N. (2010). Optical coherence tomography using a soliton pulse train, *in* Kawabe, Y. & Kawase, M. eds., *Polymer Photonics, and Novel Optical Technologies*, PWC Publishing, Chitose, Japan, pp. 116–119.

Zolla, F., Renversez, G., Nicolet, A., Kuhlmey, B., Guenneau, S. & Felbacq, D. (2005). *Foundations of Photonic Crystal Fibres*, Imperial College Press, London.

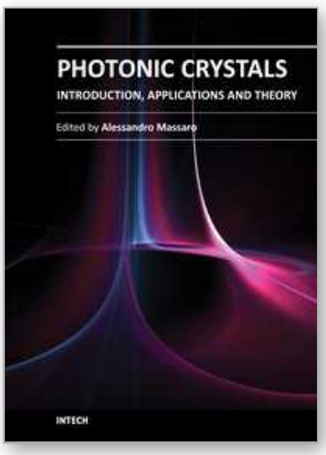

Photonic Crystals - Introduction, Applications and Theory

Edited by Dr. Alessandro Massaro

ISBN 978-953-51-0431-5
Hard cover, 344 pages
Publisher InTech
Published online 30, March, 2012
Published in print edition March, 2012

The first volume of the book concerns the introduction of photonic crystals and applications including design and modeling aspects. Photonic crystals are attractive optical materials for controlling and manipulating the flow of light. In particular, photonic crystals are of great interest for both fundamental and applied research, and the two dimensional ones are beginning to find commercial applications such as optical logic devices, micro electro-mechanical systems (MEMS), sensors. The first commercial products involving two-dimensionally periodic photonic crystals are already available in the form of photonic-crystal fibers, which use a microscale structure to confine light with radically different characteristics compared to conventional optical fiber for applications in nonlinear devices and guiding wavelengths. The goal of the first volume is to provide an overview about the listed issues.

How to reference

In order to correctly reference this scholarly work, feel free to copy and paste the following:

Naoki Karasawa and Kazuhiro Tada (2012). Optical Solitons from a Photonic Crystal Fiber and Their Applications, Photonic Crystals - Introduction, Applications and Theory, Dr. Alessandro Massaro (Ed.), ISBN: 978-953-51-0431-5, InTech, Available from: http://www.intechopen.com/books/photonic-crystals-introduction-applications-and-theory/optical-solitons-from-a-photonic-crystal-fiber-and-their-applications

INTECH
open science | open minds

InTech Europe
University Campus STeP Ri
Slavka Krautzeka 83/A
51000 Rijeka, Croatia
Phone: +385 (51) 770 447
Fax: +385 (51) 686 166
www.intechopen.com

InTech China
Unit 405, Office Block, Hotel Equatorial Shanghai
No.65, Yan An Road (West), Shanghai, 200040, China
中国上海市延安西路65号上海国际贵都大饭店办公楼405单元
Phone: +86-21-62489820
Fax: +86-21-62489821

IntechOpen